Majorana quasiparticles of an inhomogeneous Rashba chain

Maciej M. Maśka,[1,*] Anna Gorczyca-Goraj,[1] Jakub Tworzydło,[2] and Tadeusz Domański[3,†]
[1]*Department of Theoretical Physics, University of Silesia, Katowice, Poland*
[2]*Faculty of Physics, Warsaw University, Warsaw, Poland*
[3]*Institute of Physics, M. Curie-Skłodowska University, Lublin, Poland*
(Received 18 September 2016; revised manuscript received 19 December 2016; published 30 January 2017)

We investigate the inhomogeneous Rashba chain coupled to a superconducting substrate, hosting the Majorana quasiparticles near its edges. We discuss its subgap spectrum and study how robust the zero-energy quasiparticles are against the diagonal and off-diagonal disorder. Studying the $\mathbb{Z}_2$ topological invariant we show that disorder-induced transition from the topologically nontrivial to trivial phases is manifested by characteristic features in the spatially resolved quasiparticle spectrum at zero energy. We provide evidence for the nonlocal nature of the zero-energy Majorana quasiparticles that are well preserved upon partitioning the chain into separate pieces. Even though the Majorana quasiparticles are not completely immune to inhomogeneity, we show that they can spread onto other (normal) nanoscopic objects via the proximity effect.

DOI: 10.1103/PhysRevB.95.045429

I. INTRODUCTION

Quasiparticles induced at the edges of spinless (p-wave) superconducting samples in one or two dimensions have the exotic character of zero-energy bound states [1–3]. These emergent Majorana-type objects have been predicted in various systems, such as topological insulators [4,5], semiconducting nanowires [6,7], ferromagnetic chains coupled to s-wave superconducting reservoirs [8], etc. Their possible realizations have been also considered in topological superconductors with electrostatic defects [9], Josephson-type junctions [10], quantum dot chains [11–13], noncentrosymmetric superconductors [14], ultracold atom systems [15], and many others. Intensive studies of the Majorana quasiparticles have been reviewed by several authors [16–21].

The most convincing experimental evidence for the zero-energy Majorana modes have been provided so far by the tunneling measurements using the nanoscopic chains proximity coupled to the s-wave superconducting reservoirs [22–25]. The Majorana quasiparticles are driven at the edges of such chains by the strong spin-orbit coupling in the presence of the Zeeman splitting, when the induced pairing evolves into the topologically nontrivial p-wave superconductivity of identical spin electrons on the neighboring sites [6,7].

Empirical signatures of the zero-energy quasiparticles have been seen in the subgap spectroscopy. The first indication was an enhancement of the zero-bias differential conductance of the tunneling current flowing through the end states of InSb nanowire placed between the conducting (Au) electrode and the classical (Nb) superconductor [22]. The same effect has been later on reported in STM-type configuration, by measuring the spatially resolved differential conductance of magnetic (Fe) atom chain deposited on the superconducting (Pb) substrate [23,24]. Similar STM setup has been recently employed using the superconducting tip [25]. Another evidence for the Majorana modes has been reported in $Bi_2Te_3/NbSe_2$ heterostructure by means of the spin-resolved Andreev spectroscopy [26].

The purpose of our work is to study a stability of the zero-energy Majorana modes in STM-type configuration (Fig. 1), relevant to the experiments of Princeton [23] and Basel [24] groups. In realistic situations the Rashba chain on a surface of s-wave superconductor could be affected by inhomogeneity of (i) atom energies (diagonal disorder), (ii) coupling to the superconducting substrate (off-diagonal disorder), and (iii) intersite hopping integral. It is hence important to study how robust are the Majorana modes to various disorders. Some aspects of the inhomogeneous Rashba chains have been already addressed by several groups [27–40], emphasizing that the Majorana quasiparticles are not completely immune to the moderate and strong disorder [37]. Here we revisit this issue in a systematic way. In particular, we (i) study the boundary effects and their influence on spatial extent of the zero-energy bound states, (ii) consider disordered-induced transition from the topologically nontrivial to trivial states, (iii) analyze stability of the Majorana quasiparticles upon partitioning the chain into pieces, and (iv) present how the Majorana quasiparticles spread on other side-attached nanoobjects (quantum impurities) via the proximity effect.

The paper is organized as follows. In Sec. II we formulate the microscopic model and discuss the subgap spectrum of a finite-length Rashba chain. In Sec. III we consider stability of the Majorana states in the inhomogeneous chain against the random atom energies and coupling to the superconducting substrate. Next, in Sec. IV, we consider an interplay between the single impurities and the Majorana states. Finally, in Sec. V, we summarize our results, and then we present some technical details in Appendixes A–D.

II. MICROSCOPIC MODEL

Scanning tunneling microscope (STM) configuration [23,24] (displayed in Fig. 1) can be modeled by the following Hamiltonian,

$$\hat{H} = \hat{H}_{\rm tip} + \hat{H}_{\rm chain} + \hat{H}_S + \hat{V}_{\rm hybr}, \tag{1}$$

where $\hat{H}_{\rm tip}$ describes the normal tip, $\hat{H}_{\rm chain}$ refers to the atomic chain, and $\hat{H}_S$ stands for the s-wave superconducting

*maciej.maska@phys.us.edu.pl
†doman@kft.umcs.lublin.pl

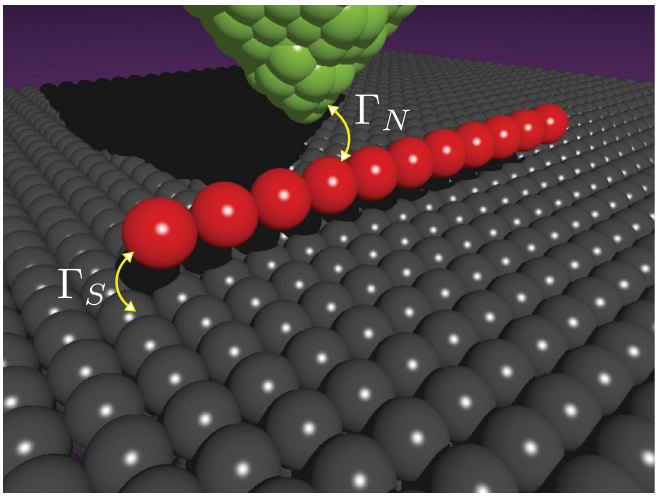

FIG. 1. Schematic view of the STM setup, in which the atomic chain (hosting the Majorana quasiparticles) is deposited on the s-wave superconducting substrate and is probed by the charge current of the normal (conducting) tip.

substrate. For specific considerations we describe the atomic chain by the tight-binding model $\hat{H}_{\rm chain} = \sum_{i,\sigma} \varepsilon_i \hat{d}^\dagger_{i,\sigma}\hat{d}_{i,\sigma} + \sum_{i,j,\sigma} t_{ij}\hat{d}^\dagger_{i,\sigma}\hat{d}_{j,\sigma} + \hat{H}_{\rm Rashba} + \hat{H}_{\rm Zeeman}$, where the second quantization operator $\hat{d}^{(\dagger)}_{i,\sigma}$ annihilates (creates) an electron at ith site with energy ε_i and spin σ, and the intersite hopping integral is denoted by t_{ij}. We assume the magnetic field $\mathbf{B} = (0,0,B)$ and the spin-orbit vector $\boldsymbol{\alpha} = (0,0,\alpha)$. We express the Rashba interaction and the Zeeman terms by

$$\hat{H}_{\rm Rashba} = -\alpha \sum_{i,\sigma,\sigma'} [\hat{d}^\dagger_{i+1,\sigma}(i\sigma^y)_{\sigma\sigma'}\hat{d}_{i,\sigma'} + \text{H.c.}], \tag{2}$$

$$\hat{H}_{\rm Zeeman} = \frac{g\mu_{\rm B}B}{2} \sum_{i,\sigma,\sigma'} \hat{d}^\dagger_{i,\sigma}(\sigma^z)_{\sigma\sigma'}\hat{d}_{i,\sigma'}. \tag{3}$$

We treat the STM tip as the free fermion gas $\hat{H}_N = \sum_{\mathbf{k},\sigma} \xi_{\mathbf{k}N}\hat{c}^\dagger_{\mathbf{k}\sigma N}\hat{c}_{\mathbf{k}\sigma N}$ and describe the isotropic superconductor by the BCS model $\hat{H}_S = \sum_{\mathbf{k},\sigma} \xi_{\mathbf{k}S}\hat{c}^\dagger_{\mathbf{k}\sigma S}\hat{c}_{\mathbf{k}\sigma S} - \sum_{\mathbf{k}} \Delta_{sc}(\hat{c}^\dagger_{\mathbf{k}\uparrow S}\hat{c}^\dagger_{-\mathbf{k}\downarrow S} + \hat{c}_{-\mathbf{k}\downarrow S}\hat{c}_{\mathbf{k}\uparrow S})$. The operators $\hat{c}^{(\dagger)}_{\mathbf{k}\sigma\beta}$ refer to the itinerant electrons with momentum $\mathbf{k}$, spin σ, and energy $\xi_{\mathbf{k}\beta} = \varepsilon_{\mathbf{k}} - \mu_\beta$ (where $\beta = N,S$). Hybridization between the atoms and both external reservoirs is described $\hat{V}_{\rm hybr} = \sum_{\mathbf{k},\sigma,\beta} (V_{i,\mathbf{k}\beta}\,\hat{d}^\dagger_{i,\sigma}\hat{c}_{\mathbf{k}\sigma\beta} + V^*_{i,\mathbf{k}\beta}\hat{c}^\dagger_{\mathbf{k}\sigma\beta}\hat{d}_{i,\sigma})$, where $V_{i,\mathbf{k}\beta}$ are the tunneling matrix elements.

A. Deep subgap regime

Since the zero-energy modes are formed inside the superconducting energy regime $(-\Delta_{sc},\Delta_{sc})$ it is convenient to introduce the characteristic couplings $\Gamma_{i,\beta} = 2\pi \sum_{\mathbf{k}} |V_{i,\mathbf{k}\beta}|^2\, \delta(\omega - \xi_{\mathbf{k}\beta})$ and treat them as constant quantities. In the weak coupling limit, $\Gamma_S \ll \Delta$, the superconducting reservoir induces the electron pairing at each of the atoms (see Appendix A for details):

$$\hat{H}_S + \sum_{\mathbf{k},\sigma} (V_{i,\mathbf{k}S}\,\hat{d}^\dagger_{i,\sigma}\hat{c}_{\mathbf{k}\sigma S} + \text{H.c.}) \equiv \Delta_i \hat{d}^\dagger_{i,\uparrow}\hat{d}^\dagger_{i,\downarrow} + \text{H.c.} \tag{4}$$

The proximity-induced pairing potential is $\Delta_i = \Gamma_{i,S}/2$. The atomic chain can be hence formally described by the following low-energy Hamiltonian [18]

$$\hat{H}^{(\rm prox)}_{\rm chain} = \sum_{i,\sigma} \varepsilon_i \hat{d}^\dagger_{i,\sigma}\hat{d}_{i,\sigma} + \sum_{i,j,\sigma} t_{ij}\hat{d}^\dagger_{i,\sigma}\hat{d}_{j,\sigma} + \hat{H}_{\rm Rashba} + \hat{H}_{\rm Zeeman} + \sum_i \Delta_i(\hat{d}^\dagger_{i,\uparrow}\hat{d}^\dagger_{i,\downarrow} + \hat{d}_{i,\downarrow}\hat{d}_{i,\uparrow}). \tag{5}$$

In a homogeneous system ($\varepsilon_i = \mu$, $t_{ij} = t\delta_{|i-j|,1}$, $\Delta_i = \Delta$) the zero-energy quasiparticles of (5) exist in the topologically nontrivial superconducting state, in a region restricted by the boundaries [6,7,41]

$$(\mu \pm 2t)^2 + \Delta^2 - V_{\rm Z}^2 = 0, \tag{6}$$

where $V_{\rm Z} = g\mu_{\rm B}B/2$ is the Zeeman energy. Majorana-type quasiparticles of the inhomogeneous systems (for various kinds of disorder) are discussed in Sec. III.

Obviously this heuristic scenario (5) does not capture any electronic states existing outside the energy gap of bulk superconductor $|\omega| > \Delta_{sc}$. To take them into account one should properly treat the dynamic effects [27,42] appearing in the energy-dependent self-energy (mentioned in Appendix A). Other possibility would be to study the Rashba chain along with the piece of superconducting substrate by the Bogoliubov–de Gennes approach [43]. Such states would eventually induce a continuous background of the high-energy spectrum, and could show up in the tunneling characteristics at $e|V| \geqslant \Delta_{sc}$. The Rashba chain weakly coupled to superconducting substrate subgap states is at low energies reliably reproduced by the static approximation (5) [18]. Our present study is focused here on stability of the zero-energy quasiparticles; therefore we skip the high-energy effects.

B. Intrinsic inhomogeneity of atomic chain

Let us briefly analyze the in-gap quasiparticles of the uniform chain consisting of N atoms. We have determined numerically the eigenvalues and eigenvectors of the proximized atomic chain (5) for $N = 70$, using the following model parameters: $\varepsilon_i/t = -2.1$, $\alpha/t = 0.15$, and $\Gamma_{i,S}/t = 0.2$. These parameters are chosen to guarantee that the system is in a topologically nontrivial regime, unless the critical disorder is achieved.

In the popular Kitaev model the Majorana bound states appear at the very last sites of a one-dimensional chain characterized by the uniform intersite triplet pairing. In reality, however, a magnitude of the induced p-wave pairing would be affected by the finite atomic length. To get some insight into such effects we investigate the pairing amplitudes of both the singlet $\langle\hat{d}_{i,\downarrow}\hat{d}_{i,\uparrow}\rangle$ and equal-spin channels $\langle\hat{d}_{i,\sigma}\hat{d}_{i+1,\sigma}\rangle$, respectively. Figure 2 shows their spatial variation for the chosen model parameters. The internal chain sites are characterized by nearly constant (uniform) value of the pairing amplitude, whereas at the edges there appear some deviations. The maximal amplitude of $\langle\hat{d}_{i,\downarrow}\hat{d}_{i,\uparrow}\rangle$ corresponds to $i \sim 3$ (and $i \sim N-3$). The other peripheral chain atoms $i = 1,2$ are characterized by the clearly reduced pairing amplitude. This intrinsic inhomogeneity has noticeable implications on the induced p-wave pairing and such aspect distinguishes

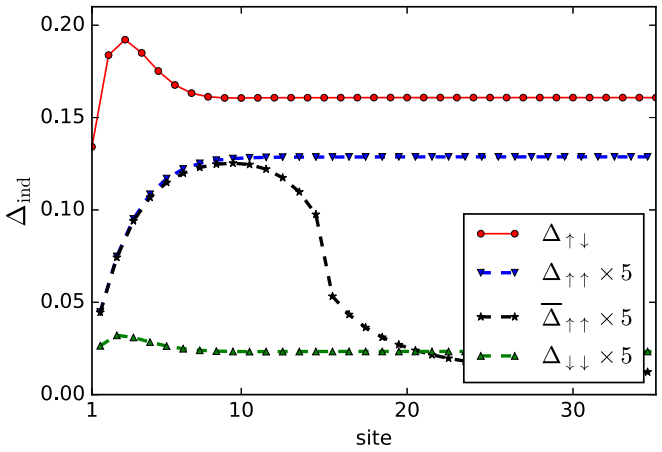

FIG. 2. The spatially resolved induced pairings $\Delta_{\uparrow\downarrow} = \langle \hat{d}_{i,\downarrow}\hat{d}_{i,\uparrow}\rangle$, $\Delta_{\uparrow\uparrow} = \langle \hat{d}_{i,\uparrow}\hat{d}_{i+1,\uparrow}\rangle$, and $\Delta_{\downarrow\downarrow} = \langle \hat{d}_{i,\downarrow}\hat{d}_{i+1,\downarrow}\rangle$ obtained for the same model parameters as in Fig. 16 and $g\mu_B B/2 = 0.27t$. $\overline{\Delta}_{\uparrow\uparrow}$ denotes the magnitude of the order parameter $\langle \hat{d}_{i,\uparrow}\hat{d}_{i+1,\uparrow}\rangle$ calculated in the case when the spin-orbit interaction is nonzero only close to the ends of the chain (on sites from 1 to 15 and from 56 to 70). For the sake of visibility the intersite equal-spin pairing amplitudes are multiplied by 5.

our approach from the Kitaev toy model [1]. Practically, such effects could be verified by means of the spin-polarized Andreev spectroscopy [26].

Spatial profile of the Majorana quasiparticles is essentially dependent on the anomalous spectral densities $\mathcal{F}_{ij\sigma\sigma'}(\omega) = -\frac{1}{\pi}\mathrm{Im}\langle\langle \hat{d}_{i,\sigma}; \hat{d}_{j,\sigma'}\rangle\rangle$ at zero energy. Figure 3 shows them for the s-wave (where $j = i$ and $\sigma \neq \sigma'$) and the p-wave (where $j = i+1$ and $\sigma = \sigma'$) pairing channels. In both cases the

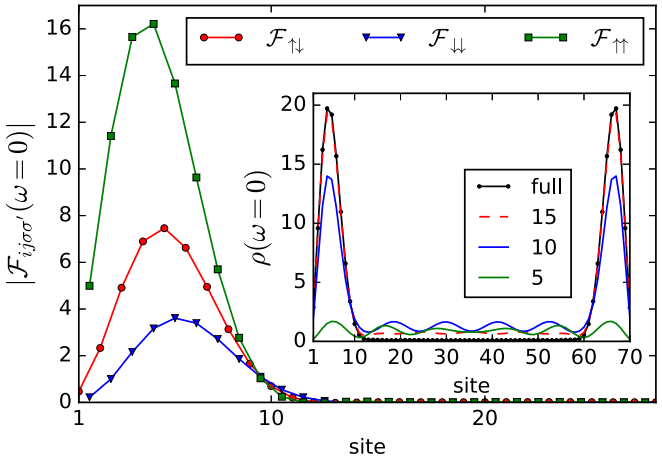

FIG. 3. Off-diagonal spectral densities $\mathcal{F}_{ij\sigma\sigma'}(\omega)$ at $\omega = 0$ for different pairings. The inset shows a comparison of the zero-energy local density of states for different sizes of the part of the chain where the spin-orbit interaction is switched off. The solid black line ("full") represents the reference chain with the spin-orbit interaction on all lattice sites. Lines described as "15," "10," and "5" show the local density of states (LDOS) in cases when the interaction is present only on 15, 10, and 5 outermost sites, respectively. Note that the line marked as "15" differs from the reference line only in the central region.

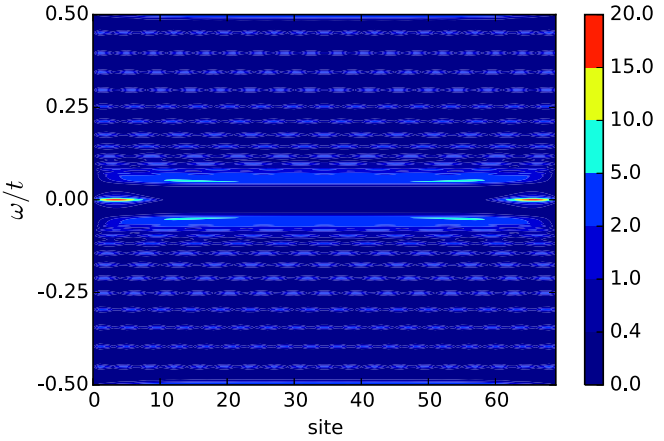

FIG. 4. Subgap spectrum of the atomic chain for each site $i \in \langle 1,70\rangle$ with the line broadening imposed by $\Gamma_N = 0.1\Gamma_S$.

anomalous spectral function $\mathcal{F}_{ij\sigma\sigma'}(\omega=0)$ does not vanish only in such regions where the Majorana states exist. The induced amplitudes (for each pairing channel shown in Fig. 2) have been calculated from $\langle \hat{d}_{i,\sigma}\hat{d}_{j,\sigma'}\rangle = \int d\omega\, \mathcal{F}_{ij\sigma\sigma'}(\omega)\, f(\omega,T)$, where $f(\omega,T) = [1+\exp(\omega/k_BT)]^{-1}$ is the Fermi-Dirac distribution function.

Since the spectral functions $\mathcal{F}_{ij\sigma\sigma'}(\omega = 0)$ vanish away from the Majorana states, we presume that electron pairing would be necessary only at the chain edges. We checked such a possibility by switching off the spin-orbit interaction (responsible for p-wave pairing) on internal sites of the chain. Our results (see inset in Fig. 3) prove that as long as the region of the absent spin-orbit interaction does not coincide with the Majorana quasiparticles, their profile is not really much affected. For instance, the red dashed line in the inset in Fig. 3 (corresponding to the spin-orbit interaction present only in 15 sites at the chain edges) is nearly identical with the result for uniform system. By further expanding the region of absent spin-orbit interaction, the Majorana states become eventually damped. Simultaneously we observe small oscillations of $\rho(\omega = 0)$ appearing in part of the atomic chain where the spin-orbit coupling is absent. This is consistent with the results reported in Ref. [38], for the Rashba chain with nonuniform spin-orbit coupling. By switching off the spin-orbit coupling in a half of the chain, the Majorana quasiparticle of the noninteracting half evolved into the finite-energy Shiba-Andreev states. Our system can be regarded as two pieces of such chains, interconnected by the noninteracting parts with two Majorana quasiparticles preserved at the opposite edges. Another relative situation will be discussed in Sec. IV, where we consider a gradual partitioning of the atomic chain.

The boundary effects have also influence on a profile of the Majorana quasiparticles [44,45]. In Fig. 4 we present the spatially resolved local density of states (LDOS). The Majorana quasiparticles spread over nearly 10 peripheral atoms and (for the chosen model parameters) their maximal intensity occurs at sites $i = 4$ and $i = 66$. This fact nicely coincides with the real experimental data, reported by the Princeton group [23]. The strongest zero-bias enhancement of the subgap STM tunneling corresponds to the point 2 in Fig. 4 of the report by Yazdani [46]. Its distance from the

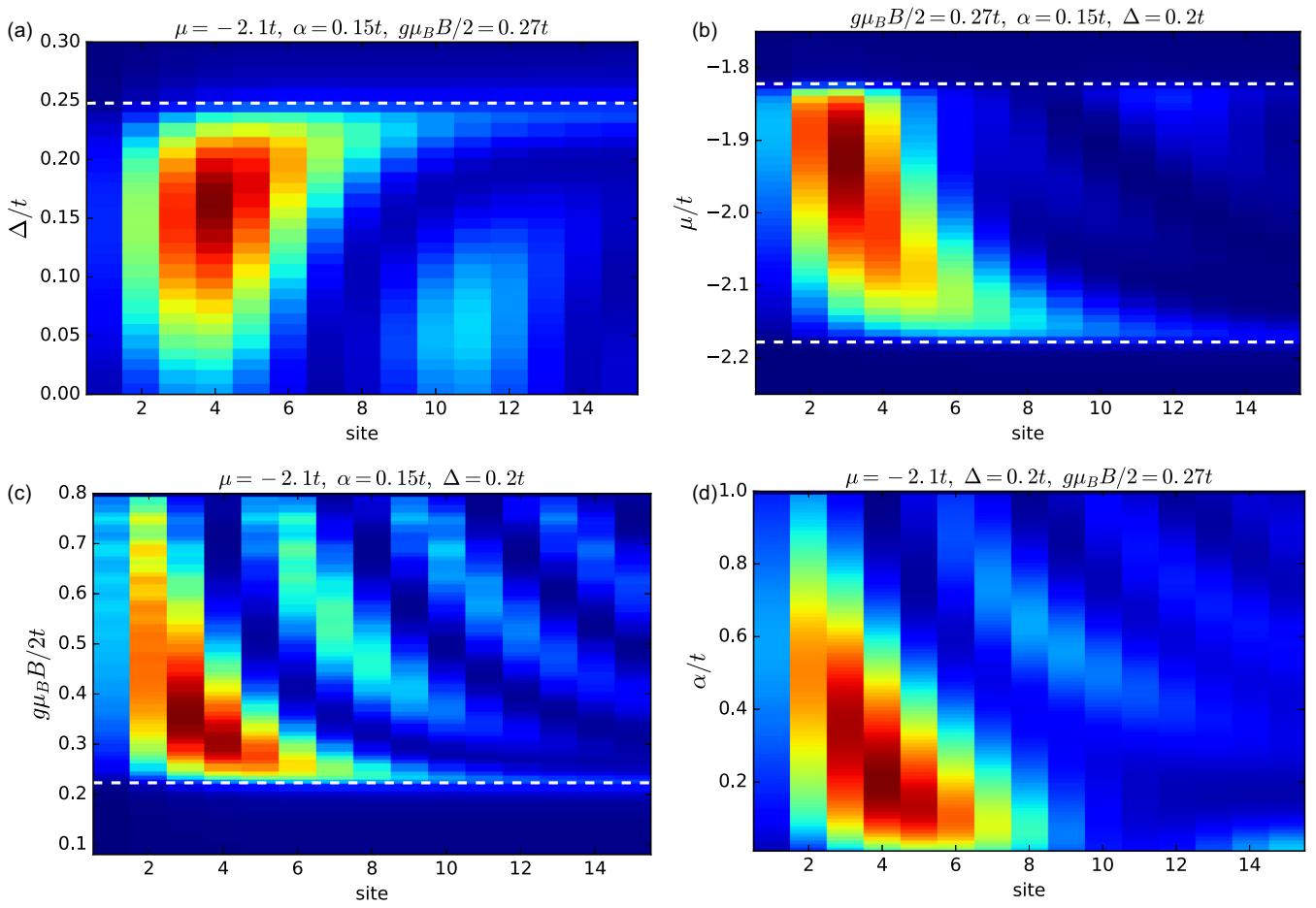

FIG. 5. Local DOS at $\omega = 0$ as a function of the model parameters: (a) magnitude of the induced pairing Δ, (b) the chemical potential μ, (c) magnetic field B, and (d) the spin-orbit coupling α. The values of the other (fixed) parameters are given above each panel. The white dashed lines show boundaries of the topological region given by Eq. (6). Note that independent of the model parameters the LDOS maximum is always shifted from the nanowire edge.

chain edge is roughly ∼8 Å, so the Majorana feature is indeed centered near the fourth iron atom.

We have checked that such maximum of the local density of states rather weakly depends on the model parameters [provided that the system is in the topologically nontrivial regime given by Eq. (6)]. Spatial profile of the zero-energy Majorana quasiparticles and their dependence on Δ, μ, B, and α are presented in Fig. 5. We clearly notice that the maximal intensity roughly appears either at the fourth or third atom from the chain edge.

LDOS at zero energy is also sensitive to the localization length of the Majorana quasiparticles and the interference between different components of the composite wave function [47–50],

$$\Psi^M(x) \sim \sin(k_F x) e^{-x/\xi}, \tag{7}$$

where k_F depends on microscopic parameters, such as the chemical potential or the Zeeman splitting. The localization length ξ itself, however, is not sufficient to explain the position of the LDOS maximum. For example, the actual maximum slightly departs from the chain edge upon increasing Δ [see Fig. 5(a)], whereas the localization length is expected to scale in the opposite way $\xi \propto 1/\Delta$ [42]. This suggests that the boundary effects within the low-energy effective model (5) describe the realistic situation, without any need for fine-tuning to reproduce the experimentally observed shape of the Majorana bound states.

III. DISORDERED RASHBA CHAIN

In this section we investigate whether the Majorana quasiparticles can sustain such forms of the inhomogeneity as the random site energies ε_i (we call it "diagonal disorder") and the spatially varying coupling $\Gamma_{i,S}$ to s-wave superconducting substrate that affects the pairing potential Δ_i (we call it "off-diagonal disorder").

A. Random site energies

We have chosen the energies $\varepsilon_i = \varepsilon + \xi_i\,\delta$ with a random number $\xi_i \in \langle -1, 1\rangle$ and the magnitude δ ranging from small to large values [38]. We have next determined the spectral function and averaged it roughly over $\sim 10^4$ different configurations $\{\xi_i\}$, depending on δ. The main panel in Fig. 6 displays spatial variation of the averaged spectral function at zero energy $\omega = 0$ for representative values of δ, ranging from the weak to strong disorder.

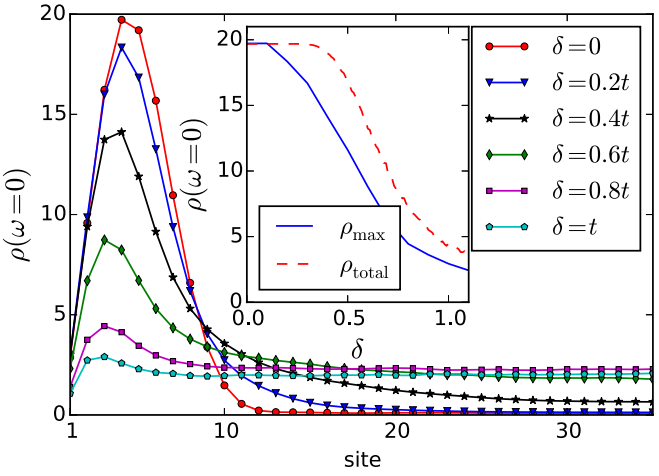

FIG. 6. Evolution of the zero-energy subgap quasiparticle spectrum $\rho_i(\omega=0)$ driven by the diagonal disorder. Inset shows the local density of states obtained at $\omega=0$ for $i=4$, where the Majorana quasiparticle has the highest probability (solid blue line) and the density of states averaged over all sites of the chain (rescaled to the same maximum value, dashed red line).

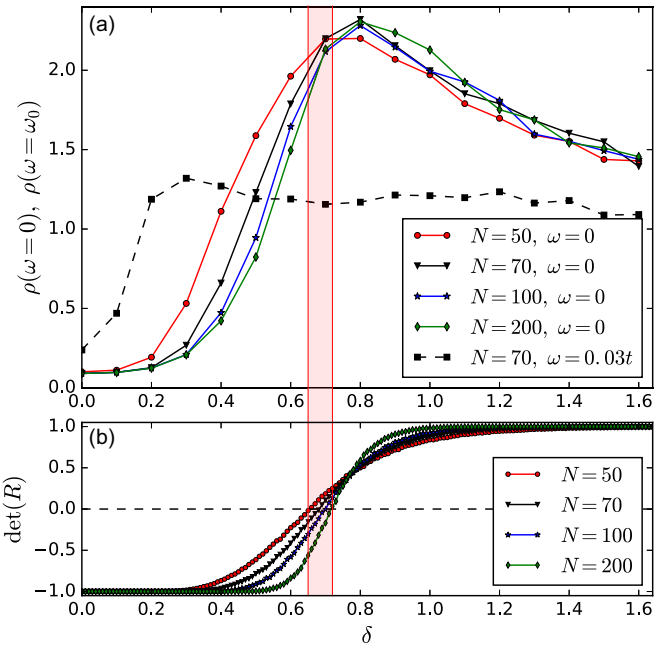

FIG. 7. The quasiparticle spectrum $\rho_i(\omega)$ at the central site $i=N/2$ averaged over 10^4 realizations of the random site energies. The solid lines in panel (a) show the density of states at $\omega=0$ for several N, as indicated. The black dashed line presents $\rho_i(\omega_0)$ at small (yet finite) energy $\omega_0=0.03t$ for $N=70$. Panel (b) presents the determinant of the reflection matrix averaged over 10^3 disorder realizations versus the disorder δ. Sign of this determinant changes between the topologically trivial and nontrivial phases, as discussed in Sec. III C. The vertical stripe marks a range of δ in which the averaged $\det(R)$ changes the sign, depending on the chain length varying from $N=50$ to $N=200$. We can notice that the sign change of $\det(R)$ nearly coincides with the maximum of $\rho_i(\omega=0)$.

With increasing δ the subgap spectrum is gradually filled in. To illustrate this behavior we present in inset to Fig. 6 the spectral function $\rho_i(\omega=0)$ at site $i=4$ (solid blue line), where the Majorana quasiparticle has the largest probability. We observe that near some critical amplitude $\delta^*\sim 0.7$ our system undergoes a qualitative changeover, above which $\rho_4(\omega=0)$ asymptotically tends to a value common for the entire atomic chain. The dashed red line in inset to Fig. 6 shows the density of states averaged over entire chain. We can notice that for a weak disorder the averaged zero-energy density remains almost intact. It means that in the presence of the weak disorder the bound states survive at $\omega=0$, but they can be shifted from the chain edges. For stronger disorder the total zero-energy density is reduced, indicating that the subgap quasiparticles move to finite energies.

To further clarify such changeover we show in Fig. 7 concomitant evolution of the averaged spectral function $\rho_i(\omega=0)$ at the internal site $i=N/2$ (where for $\delta=0$ the zero-energy quasiparticles are absent). With increasing disorder (but below δ^*) the zero-energy states gradually build up. We argue that they originate from the Majorana states that are pinned by disorder on internal sites (as explained in Sec. IV). With further increase of δ (above δ^*) the zero-energy spectral function slowly diminishes. This tendency is caused by evolution from the nontrivial to trivial superconducting phases. Such changeover is smooth, regardless of the atomic chain size N (see the solid lines in Fig. 7). Additional indication that strong disorder triggers the trivial superconducting state is provided by evolution of $\rho_i(\omega)$ at finite energy $\omega=0.03t$, corresponding to the soft gap regime (see Appendix B). The black dashed line in Fig. 7 indeed shows that strong disorder closes the soft gap, which is evidenced by saturation of $\rho_i(\omega=0.03t)$ for large δ, inducing the ordinary Andreev-Shiba states. A similar scenario, where the Majorana quasiparticles are destroyed by critical disorder, holds true also for more realistic multiband systems (see Appendix D). Additional evidence that the critical disorder magnitude δ^* corresponds to transition to the topologically trivial phase is provided in Sec. III C.

There is a significant advantage of studying the local density of states away from the Majorana edge states. As illustrated in Fig. 6, the magnitude of the Majorana states smoothly decreases almost to zero with increasing disorder without any characteristic points that could be used to pinpoint the topological transition. However, in the corresponding evolution of the zero-energy states away from the chain edges (Fig. 7), such a feature is well pronounced and can be easily identified.

Figure 8 illustrates the zero-energy p-wave spectral density versus δ obtained for various N. This result confirms that above δ^* the Majorana quasiparticles disappear as a consequence of the suppressed equal-spin pairing and δ^* can be regarded to be characteristic point for a crossover to the nontrivial pairing.

It is interesting that for $\delta<\delta^*$ the spectral function $\rho_i(\omega=0)$ scales with the system size N, whereas only minor statistical fluctuations show up above δ^*. While for any finite disorder all the states are localized (what is seen by means of the *inverse participation ratio* method, not presented here), it may suggest that at δ^* the localization length changes abruptly. The critical character of δ^* is even more pronounced in the geometrically averaged local density of states (see Appendix C).

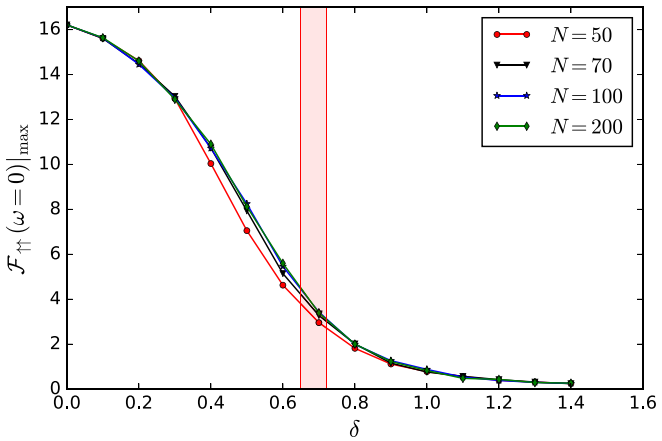

FIG. 8. Suppression of the p-wave superconducting phase induced by the disorder, where $\mathcal{F}_{\uparrow\uparrow}(\omega=0)|_{\max}$ is the maximum of the p-wave spectral density along the chain. The red vertical strip has the same meaning as in Fig. 7(b).

B. Random coupling to superconducting substrate

In analogy to the random site energies (discussed in previous subsection) we have studied the inhomogeneous coupling between the chain atoms and superconducting substrate $\Gamma_{i,S} = \Gamma_S + \xi_i\,\delta$. Physically such situation may occur when the wave functions of atoms randomly overlap with the wave functions of itinerant electrons in superconducting substrate. This kind of disorder (that appears in off-diagonal Green's function of the Nambu representation) is known to have detrimental influence on superconductivity of bulk materials [51].

Figure 9 shows the results obtained for several amplitudes δ (in units of t) of the off-diagonal disorder imposed on the reference value $\Gamma_S/t = 0.2$. We roughly observe a similar tendency as in Fig. 6, but a more careful examination indicates that nonuniform coupling $\Gamma_{i,S}$ is slightly less influential on the Majorana quasiparticles [38].

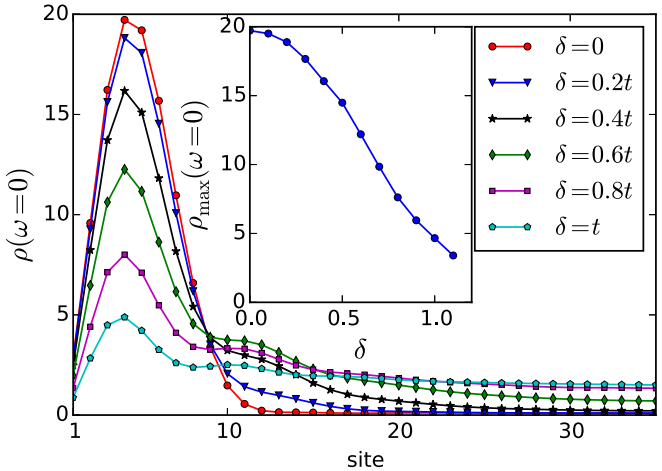

FIG. 9. Evolution of the subgap quasiparticle spectrum $\rho_i(\omega=0)$ caused by the random coupling $\Gamma_{i,S}$.

C. Topological quantum number

So far we have analyzed evolution of the local density of states at $\omega = 0$, providing indirect evidence for the disorder-induced destruction of the Majorana bound states. We argued that transfer of the averaged spectral density $\rho(\omega)$ from the chain ends to its internal lattice sites (below some critical δ^*) was caused by pinning of the Majorana states by disorder. For stronger $\delta > \delta^*$ the Majorana states disappeared and the quasiparticle peaks moved to finite (nonzero) energies. In consequence the averaged $\rho(\omega=0)$ decreased and its maximal value (located at the central chain sites) indicated a smooth transition to the topologically trivial superconducting phase. In order to check whether this interpretation of transition from the topologically nontrivial to trivial regions (at δ^*) is correct we shall analyze it here by determining the $\mathbb{Z}_2$ topological quantum number.

The topological quantum number $\mathcal{Q}$ can identify whether the chain is in the topologically trivial ($\mathcal{Q}=1$) or nontrivial ($\mathcal{Q}=-1$) state. Kitaev [1] has shown that for a translationally invariant nanowire this quantity can be expressed as $\mathcal{Q} = \operatorname{sign}\mathrm{Pf}[A(0)]\mathrm{Pf}[A(\pi)]$, where $A(k)$ is the Hamiltonian in momentum space transformed to the Majorana basis. In the disordered systems, however, skew-symmetric matrices $A(k)$ are very large so it is cumbersome to calculate $\mathcal{Q}$ from the above formula.

In Refs. [52,53] it has been shown that the topological number $\mathcal{Q}$ can be determined from the scattering matrix S of the chain

$$S = \begin{pmatrix} R & T' \\ T & R' \end{pmatrix}, \tag{8}$$

where R and T (R' and T') are 4×4 reflection and transmission matrices, respectively, at the left (right) end of the chain. This matrix describes transport through the chain coupled to left and right leads

$$\begin{pmatrix} \psi_{-,\mathrm{L}} \\ \psi_{+,\mathrm{R}} \end{pmatrix} = S \begin{pmatrix} \psi_{+,\mathrm{L}} \\ \psi_{-,\mathrm{R}} \end{pmatrix}, \tag{9}$$

where $\psi_{\pm,L/R}$ are the right or left moving modes ($\pm$) at the left or right edge (L/R) at the Fermi level. Then, the topological quantum number is given by

$$\mathcal{Q} = \operatorname{sign}\det(R) = \operatorname{sign}\det(R'). \tag{10}$$

The scattering matrix S can be obtained from multiplication of the individual transfer matrices of all the lattice sites. This procedure has been described in detailed in Ref. [8]. Since the product of numerous transfer matrices is numerically unstable, we converted them into a composition of the unitary matrices, involving only eigenvalues of unit absolute value. This stabilization method has been proposed in Ref. [54]. Figure 10 shows $\det(R)$ as a function of the chemical potential μ and magnetic field B for the uniform Rashba chain (without any disorder).

Difference between the boundaries of the topologically nontrivial regime given by Eq. (6) and the actual change of sign of $\det(R)$ results from the finite length of Rashba chain. By comparing the main plot with the inset in Fig. 10 (corresponding to 500-site chain) we clearly observe that topological properties for the model parameters (chosen in

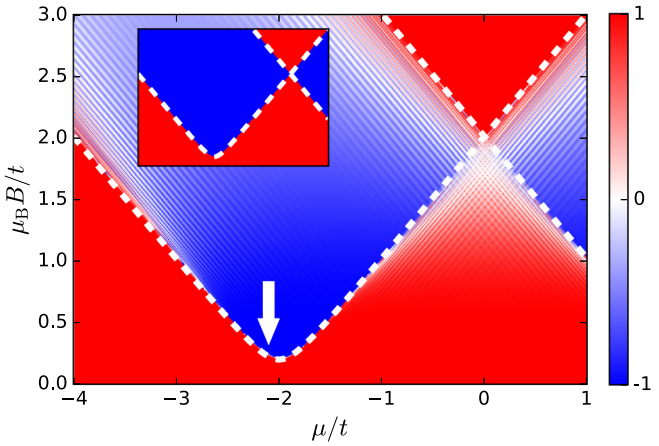

FIG. 10. det(R) as a function of the chemical potential μ and magnetic field B for a clean chain composed of 70 lattice sites. The rest of the model parameters are the same as assumed in the calculations. The white dashed lines show the boundaries of the topologically nontrivial regime given by Eq. (6). The arrow indicates the parameters used in the study of the disorder-induced destruction of the Majorana end states. The inset shows the same for a 500-site chain.

Sec. II) are only slightly smeared by the finite-size effects. In such regime the topologically nontrivial state remains intact also in presence of the weak disorder ($\delta < \delta^*$). This can be seen in Fig. 11, where we display det(R) averaged over 10^4 disorder realizations for $\delta = 0.25t$ and $\delta = 0.5t$, respectively.

A criterion based on the topological number $\mathcal{Q}$ was used by us to establish the magnitude of disorder, above which the Majorana bound states disappear. Figure 7(b) shows that such topological transition indeed takes place around δ^*. This confirms that maximum of $\rho(\omega = 0)$ in the central part of the Rashba chain coincides with the crossover between the topologically distinct phases. Above δ^* the system enters the topologically trivial phase, where the bound quasiparticle states are lifted to finite (nonzero) energies, leading to suppression of $\rho(\omega = 0)$. A closer look at Fig. 7(b) reveals that det(R) in the changeover regime is getting steeper with increasing length of the chain and that the point where it changes its sign is moving towards stronger disorder. The critical disorder δ^* in the limit of an infinite chain is indicated by the point where all the lines representing det(R) for different chain lengths cross each other. This point is very close to the maximum of $\rho(\omega = 0)$.

IV. SINGLE IMPURITIES

Another interesting situation can be caused by single impurities existing either in the Rashba chain or attached to it. We briefly address such problem in this section.

A. Splitting of the Rashba chain

Let us consider a single internal defect that can effectively produce additional pair of the Majorana quasiparticles. To be specific, we assume a reduced hopping integral t' between one pair of the internal sites in the Rashba chain. For numerical calculations we imposed the reduced hopping t' between 35th and 36th sites of the atomic chain, consisting of 70 atoms. We checked that a particular position of the reduced interatomic hopping is not crucial as long as it is well in between the Majorana quasiparticles.

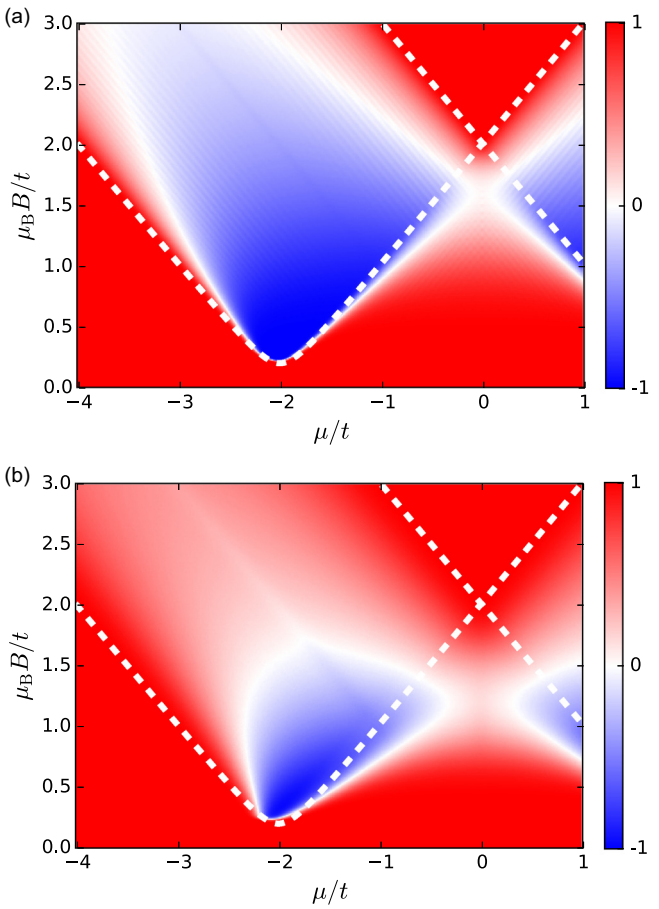

FIG. 11. The same as in Fig. 10, but in the presence of disorder with $\delta = 0.25t$ (a) and $\delta = 0.5t$ (b), respectively. Value of det(R) is averaged over 10^4 realizations of disorder. The white area separating the red and blue regions correspond to the borderline (where det(R) changes sign) between the topologically distinct phases.

In Fig. 12 we illustrate emergence of the Majorana quasiparticles driven by the suppressed hopping integral $t' < t$ (which can be regarded as a particular kind of the local defect). In the limit $t' \to 0$ the Rashba chain is decomposed into separate segments and during this process one pair of the finite-energy (Andreev) states gradually evolves into the zero-energy Majorana states. Although this phenomenon is rather obvious, it is quite astonishing that the Majorana states, already existing at the edges of uniform chain, are completely unaffected by the chain partitioning. We assign this unique behavior to nonlocal character of the edge Majorana states. This effect is similar to what we presented in Sec. II B, investigating the Majorana quasiparticles of the atomic chain in absence of the spin-orbit coupling on its interior part. Similar internal pairs of the Majorana quasiparticle states have been predicted on interface between the chain segments, where the spin-orbit coupling α changes sign [35]. The reduced hopping t' considered here seems to be quite realistic because it could explain origin of the bright spots observed near the locally deformed Fe-atom chain

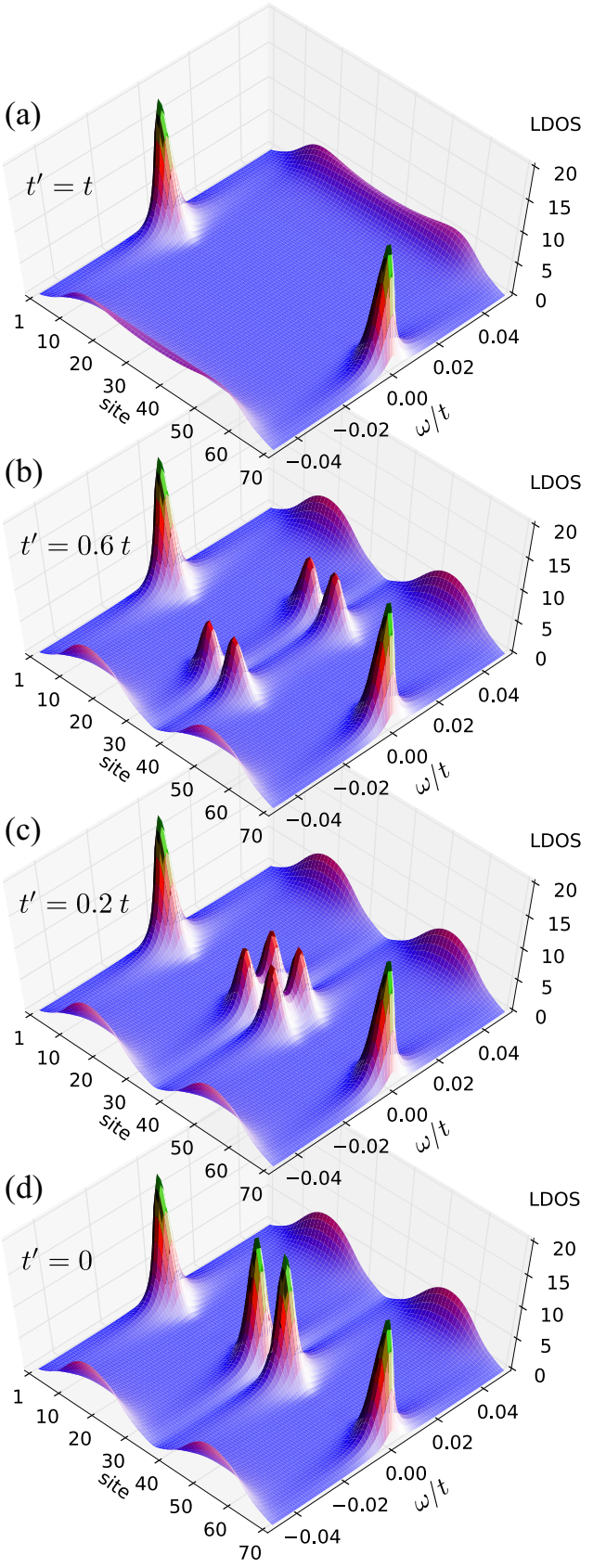

FIG. 12. The spatially and energy-dependent spectral function $\rho_i(\omega)$ of the atomic chain, where the hopping integral between the internal 35th and 36th sites is reduced to $t'/t = 1$, 0.6, 0.2, and 0 (from top to bottom).

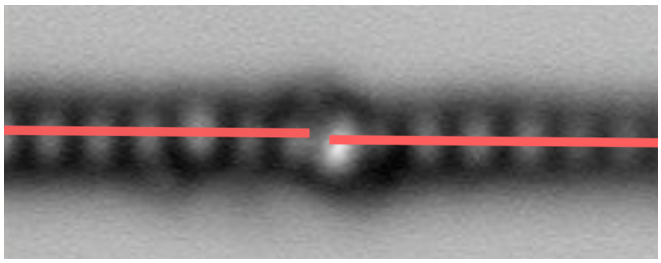

FIG. 13. Constant-height zero-bias AFM image of the Fe chain used in the Basel experiment. The red lines drawn on top of the image show that there are sections shifted in the direction perpendicular to the chain. This defect image is part of Fig. 2(c) from Ref. [24] used and modified in accordance with the Creative Commons Attribution license.

in the Basel group experiment (Fig. 13). To verify this, one should inspect the spatially resolved differential conductance measured around such defect.

B. Diagonal and off-diagonal impurity

Similar effects can be also achieved if we place either the diagonal or off-diagonal impurity in one of the internal Rashba chain sites. In practice, however, such internal impurity has to be extremely distinct from all remaining constituents of the chain. Our numerical calculations showed that the impurity potential has to be very large ($\delta > 10t$) to effectively break the chain into separate pieces, generating an additional pair of the Majorana quasiparticles. This situation is hardly probable in realistic systems; therefore we discard it from present considerations.

C. Side-attached normal impurity

Let us finally analyze what happens when a (normal) quantum impurity is coupled to the Rashba chain at the sites which host the Majorana quasiparticle. A similar issue has been previously addressed, considering the impurity coupled to the very end of Kitaev chain [43,50,55,56]. In a finite-size Rashba chain, the maximum probability of the Majorana quasiparticles does not coincide with the very last sites, but they are located around the fourth site from the atomic edge (as reported experimentally [46]). For this reason we expect the strongest influence of the Majorana quasiparticle on the normal quantum impurity when the latter is side attached to the fourth site of the Rashba chain.

On a formal level, we studied the model Hamiltonian (5) supplemented with the term

$$H_{\mathrm{imp}} = \varepsilon_f \sum_{\sigma} \hat{f}^{\dagger}_{\sigma} \hat{f}_{\sigma} + t_f \sum_{\sigma} (\hat{f}^{\dagger}_{\sigma} \hat{d}_{j,\sigma} + \mathrm{H.c.}), \qquad (11)$$

describing the quantum impurity of energy ε_f attached to site $j = 4$ of the topological wire. In Fig. 14 we present electronic spectrum of the quantum impurity $\rho_f(\omega)$ obtained for several couplings t_f/t, as indicated. With increasing t_f we observe the appearance of the zero-energy state that absorbs more spectral weight. This feature is caused by the proximity effect, which can be considered as leakage of Majorana mode onto normal quantum impurities [55,56]. As a minor remark, let us notice

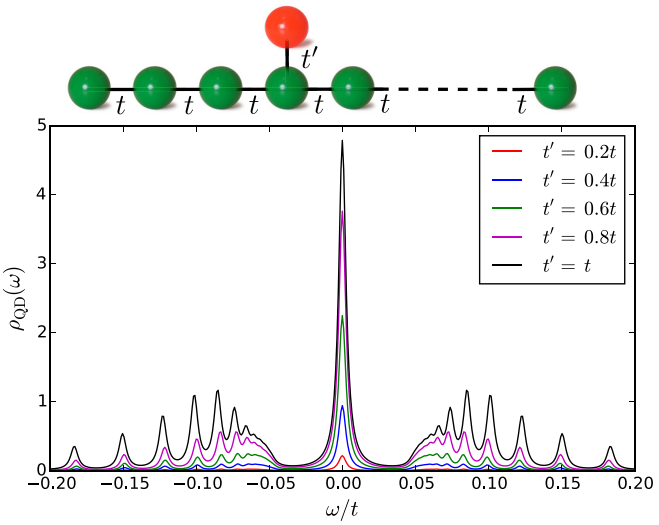

FIG. 14. The proximity effect showing up in the spectrum of the normal quantum impurity (the red sphere in the top panel) that is side-attached to the atomic chain, near the Majorana quasiparticle.

that the finite-energy (Andreev-Shiba) states do leak into the normal quantum impurity as well.

Summarizing this section, we conclude that various types of quantum impurities may play an important role for the Majorana quasiparticles of the Rashba chain. The reduced hopping integral or the strong local potential (both in the single particle and pairing channels) can effectively break the chain into pieces, so that an additional pair of Majorana quasiparticles emerges. On the other hand, any nanoscopic object coupled to the existing Majorana quasiparticle absorbs such exotic entity in exactly the same way as the superconducting or magnetic order spreading onto some neighboring normal regions.

V. SUMMARY

We studied the subgap electronic spectrum of the inhomogeneous Rashba chain deposited on s-wave superconducting substrate, where the strong spin-orbit coupling combined with the Zeeman effect induce the zero-energy Majorana quasiparticles near its edges. We analyzed the spatial extent of such quasiparticles due to intrinsic inhomogeneity caused by the boundary effects.

We also investigated stability of the Majorana quasiparticles against various types of the disorder that are likely to occur in realistic STM-type configurations (schematically displayed in Fig. 1). Despite a common belief that the Majorana quasiparticles are robust to environmental influence, we have shown that this is not truly the case. Our study reveals that sufficiently strong disorder would be detrimental for the Majorana quasiparticles, causing a transition from the topologically nontrivial to trivial superconducting phases. This conclusion is unambiguously supported by the value of the $\mathbb{Z}_2$ topological number, averaged over numerous ($\sim 10^4$) different configurations with the fixed amplitude δ. We have shown that such a qualitative changeover would be spectroscopically manifested by a peak in the zero-energy spectrum in the internal chain sites (Fig. 7). We demonstrated that this peak is present not only in a simple single-band model, but also in a more realistic multiband one.

Since it is difficult to measure the topological invariant, this effect might be useful for empirical determination of the critical disorder δ^*, signaling a transition between the nontrivial and trivial phases. It would particularly well suited for systems, where disorder can be modified in a controllable way, e.g., in ultracold atoms [57].

Single quantum impurities have also very unusual interplay with the Majorana quasiparticle states. Under specific conditions they can effectively induce additional pairs of the Majorana states, when the strong impurity scattering affects any internal site of the Rashba chain. This process is analogous to partitioning the chain into separate pieces, bringing to life new Majoranas. It is amazing, however, that the existing (external) Majorana modes are practically left intact by such partitioning. This unusual phenomenon is a signature of their nonlocal origin that could be useful for constructing the quantum bits out of Majorana quasiparticles. We also have shown that Majorana quasiparticles can spread onto nanoscopic objects coupled to them. Such proximity effect can be helpful for designing some novel tunneling heterostructures to indirectly probe the Majorana quasiparticles, for instance, by the quantum interference.

ACKNOWLEDGMENTS

We thank M. Kisiel for discussions and pointing to us signatures of the internal chain defect reported in Ref. [24]. This work is supported by the National Science Centre (Poland) under the Contracts No. DEC-2014/13/B/ST3/04451 (T.D.) and No. DEC-2013/11/B/ST3/00824 (M.M.M.).

APPENDIX A: IN-GAP STATES OF THE PROXIMIZED ATOM

To support relevance of the microscopic model (5) for the deep subgap regime ($|\omega| \ll \Delta$) let us study influence of the proximity effect on the single atom (Anderson-type impurity) placed between the normal and superconducting reservoirs, neglecting the intersite hopping $t_{ij} = 0$. Since all atoms behave identically we can skip index i when studying the spectrum of a given atom. To account for the proximity effect we have to treat the particle and hole degrees of freedom on equal footing. This can be done within the Nambu representation $\hat{\Psi}_d^\dagger = (\hat{d}_\uparrow^\dagger, \hat{d}_\downarrow)$, $\hat{\Psi}_d = (\hat{\Psi}_d^\dagger)^\dagger$ introducing the single-particle matrix Green's function $\boldsymbol{G}(\tau,\tau') = \langle\langle \hat{\Psi}_d(\tau); \hat{\Psi}_d^\dagger(\tau')\rangle\rangle$. The electronic spectrum and the transport properties (see Appendix B) are given by its diagonal and off-diagonal parts, respectively.

In equilibrium conditions ($\mu_N = \mu_S$) the Fourier transform of $\boldsymbol{G}_d(\tau,\tau') = \boldsymbol{G}_d(\tau - \tau')$ can be expressed as

$$\boldsymbol{G}^{-1}(\omega) = \begin{pmatrix} \omega - \varepsilon & 0 \\ 0 & \omega + \varepsilon \end{pmatrix} - \boldsymbol{\Sigma}_d(\omega). \tag{A1}$$

In general, the self-energy $\boldsymbol{\Sigma}_d(\omega)$ accounts for the hybridization of the quantum impurity with external reservoirs and the correlation effects. In the absence of the correlations its exact form $\boldsymbol{\Sigma}_d(\omega) = \sum_{\mathbf{k},\beta} |V_{\mathbf{k}\beta}|^2 g_{\mathbf{k}\beta}(\omega)$ depends on the Green's functions $g_{\mathbf{k}\beta}(\omega)$ of mobile electrons. In the wide-band limit

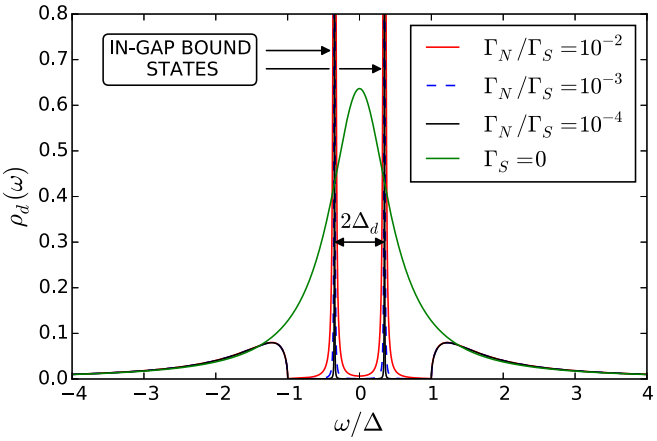

FIG. 15. Spectrum of the isolated atom ($t_{ij} = 0$) coupled to the superconducting (Γ_S) and normal (Γ_N) reservoirs. Results are obtained in the absence of the correlations for $\varepsilon = 0$, $\Delta = 2\Gamma_S$ and several coupling ratios Γ_N/Γ_S, as indicated.

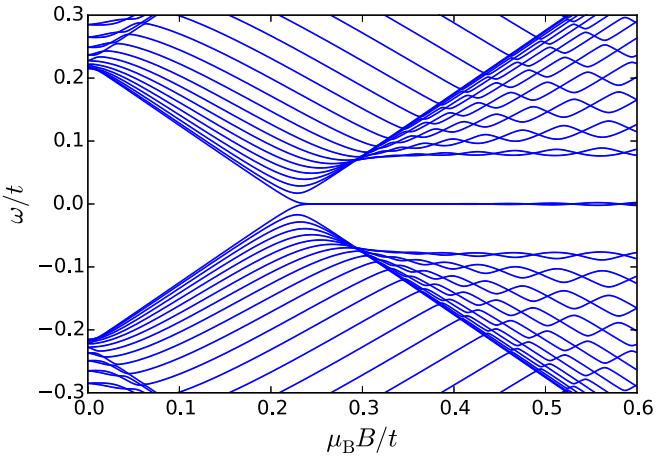

FIG. 16. Evolution of the subgap quasiparticle energies of the uniform Rashba chain from the (topologically) trivial to nontrivial superconducting phases above $B_c \approx 0.22$.

$\mathbf{\Sigma}_d(\omega)$ simplifies to [58,59]

$$\mathbf{\Sigma}_d(\omega) = -\frac{i\Gamma_N}{2}\begin{pmatrix}1 & 0\\ 0 & 1\end{pmatrix} - \frac{\Gamma_S}{2}\begin{pmatrix}1 & \frac{\Delta}{\omega}\\ \frac{\Delta}{\omega} & 1\end{pmatrix} \times \begin{cases}\frac{\omega}{\sqrt{\Delta^2-\omega^2}} & \text{for } |\omega| < \Delta\\ \frac{i\,|\omega|}{\sqrt{\omega^2-\Delta^2}} & \text{for } |\omega| > \Delta\end{cases}. \tag{A2}$$

Equation (A2) describes (i) the proximity-induced electron pairing (via the off-diagonal terms that are proportional to Γ_S) and (ii) the finite lifetime effects. The latter come from the imaginary parts of the self-energy (A2) and depend either on both couplings $\Gamma_{\beta=N,S}$ (for energies $|\omega| \gtrsim \Delta$) or solely on Γ_N (in the subgap regime $|\omega| < \Delta$).

In the subgap regime $|\omega| < \Delta$ the Green's function acquires the BCS-type structure

$$\boldsymbol{G}(\omega) = \begin{pmatrix}\tilde{\omega} + i\Gamma_N/2 - \varepsilon & \tilde{\Gamma}_S/2\\ \tilde{\Gamma}_S/2 & \tilde{\omega} + i\Gamma_N/2 + \varepsilon\end{pmatrix}^{-1} \tag{A3}$$

with $\tilde{\omega} = \omega + \frac{\Gamma_S}{2}\frac{\omega}{\sqrt{\Delta^2-\omega^2}}$ and $\tilde{\Gamma}_S = \Gamma_S\frac{\Delta}{\sqrt{\Delta^2-\omega^2}}$, respectively. The spectral function $\rho_d(\omega) = -\pi^{-1}\mathrm{Im}\boldsymbol{G}_{11}(\omega + i0^+)$ reveals two in-gap peaks, related to the Andreev [58,60] or Yu-Shiba-Rusinov [51,61] quasiparticles. We can regard their splitting as the induced pairing gap Δ_d (Fig. 15).

Figure 15 shows the spectral function for several ratios Γ_N/Γ_S. In the extreme regime $\Gamma_N \to 0$ the in-gap quasiparticles are represented by the Dirac distribution functions (i.e., their lifetime is infinite). Otherwise the broadening of in-gap states is proportional to Γ_N. Energies $E_{A,\pm}$ of the Andreev quasiparticles have to be determined from the following equation [62]:

$$E_{A,\pm} + \frac{(\Gamma_S/2)E_{A,\pm}}{\sqrt{\Delta^2 - E_{A,\pm}^2}} = \pm\sqrt{\varepsilon^2 + \frac{(\Gamma_S/2)^2\Delta^2}{\Delta^2 - E_{A,\pm}^2}}. \tag{A4}$$

For $\Gamma_S \gg \Delta$ the quasiparticle energies (A4) appear close to the superconductor gap edges $E_{A,\pm} \simeq \pm\Delta$, whereas in the weak coupling limit, $\Gamma_S \ll \Delta$, the asymptotic values are $E_{A,\pm} \simeq \pm\sqrt{\varepsilon + (\Gamma_S/2)^2}$.

In the superconducting atomic limit $\Gamma_N \to 0$ the self-energy (A2) becomes static

$$\mathbf{\Sigma}_d^0(\omega) = -\frac{1}{2}\begin{pmatrix}i\Gamma_N & \Gamma_S\\ \Gamma_S & i\Gamma_N\end{pmatrix}, \tag{A5}$$

and therefore the following equivalence holds:

$$\sum_\sigma \varepsilon\hat{d}_\sigma^\dagger\hat{d}_\sigma + \hat{H}_S + \sum_{\mathbf{k},\sigma}(V_{\mathbf{k}S}\,\hat{d}_{i,\sigma}^\dagger\hat{c}_{\mathbf{k}\sigma S} + \text{H.c.}) = \sum_\sigma \varepsilon\hat{d}_\sigma^\dagger\hat{d}_\sigma - (\Delta_d\hat{d}_\uparrow^\dagger\hat{d}_\downarrow^\dagger + \text{H.c.}) \tag{A6}$$

with $\Delta_d = \Gamma_S/2$ valid for the deep subgap regime $|\omega| \ll \Delta$. This line of reasoning allows us to represent the initial Hamiltonian (1) of the atomic chain by (5) that describes the proximized quantum wire coupled to the STM tip.

APPENDIX B: IN-GAP STATES OF THE CHAIN

In Fig. 16 we show typical variation of the in-gap quasiparticle energies versus the magnetic field B, expressed in units of $t/(g\mu_B/2)$. We notice that at some critical value ($B_c \approx 0.22$) two in-gap quasiparticles evolve into the zero-energy bound states. Because of a finite chain length there is some overlap between these Majoranas, observable by a tiny splitting of the zero-energy modes with magnitude dependent on the magnetic field. Above B_c these Majorana modes are protected by the soft gap ($\sim 0.1t$ for the present set of parameters) outside of which there exist the ordinary (Andreev-Shiba) states.

APPENDIX C: CROSSOVER TO TRIVIAL PHASE

In this section we provide additional evidence for a crossover from the nontrivial (p-wave) to trivial (s-wave) pairing driven by the diagonal disorder (random energies of the atoms). Figure 17 shows the geometrically averaged density

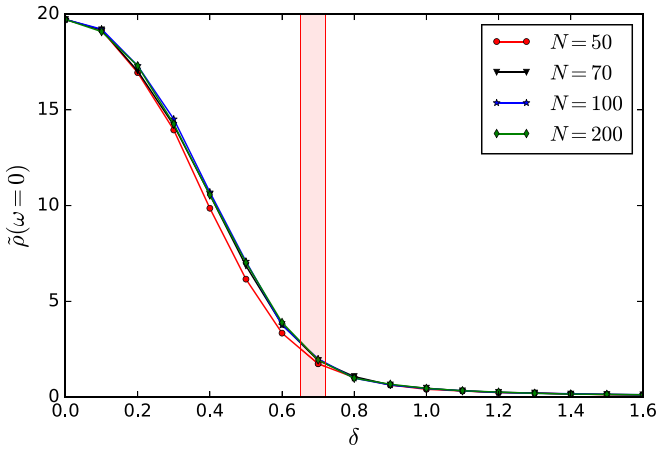

FIG. 17. Geometrically averaged density of states obtained at $\omega = 0$ for site $i = 4$ as a function of the diagonal disorder. The red vertical strip corresponds to the changeover from the nontrivial to trivial superconducting phases (as defined in Fig. 7).

of states $\tilde{\rho}_i(\omega) \equiv \exp\langle \ln \rho_i(\omega)\rangle_{\{\xi_i\}}$ (*typical density of states*) versus the disorder amplitude δ at site $i = 4$, corresponding to the maximum of the zero-energy Majorana mode. We noticed that length N has practically no effect; therefore we conclude that gradual disappearance of the Majorana quasiparticles is a generic property. Point δ^* can be interpreted as characteristic for the smooth transition from the nontrivial to trivial superconducting phases.

Figure 18 presents the geometrically averaged density of states at the central site $i = N/2$. We suspect that the weak disorder regime is related with the Majorana mode(s) which are eventually pinned at individual sites inside the chain. This process is somewhat sensitive to the atomic chain length N. On the other hand, for stronger disorder $\delta > \delta^*$, we observe the monotonous decrease of the spectral function at zero energy (that is almost insensitive to N). Using geometrical averaging we notice that the maximum of $\tilde{\rho}(\omega = 0)$ is much more pronounced than in the case of arithmetic averaging (Fig. 7). Moreover, in the present Fig. 18 the maximum perfectly coincides with the transition where the topological

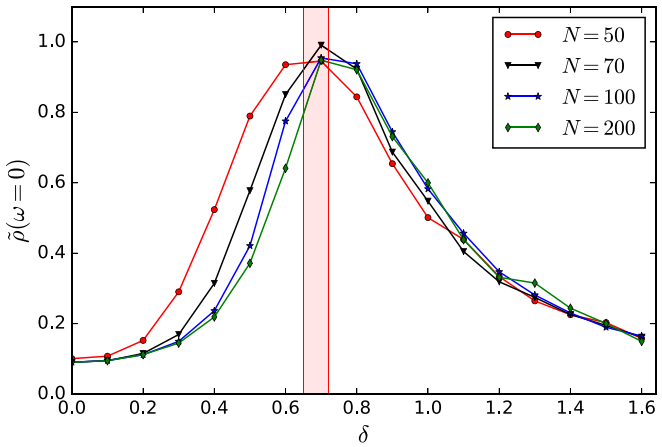

FIG. 18. Geometrically averaged local density of states obtained for $\omega = 0$ at the central site $i = N/2$. The meaning of the red vertical strip is the same as in Fig. 7).

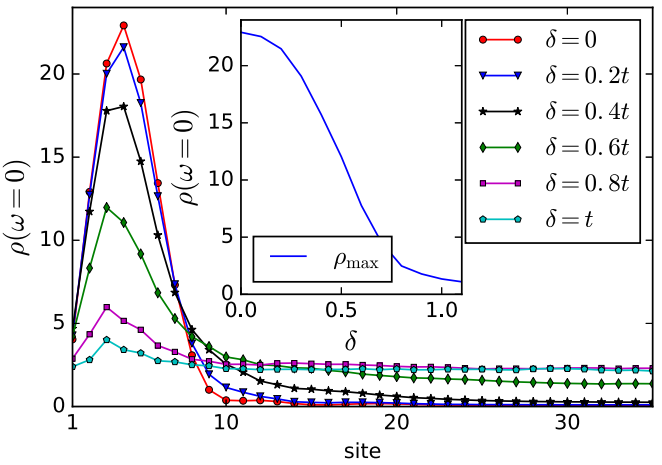

FIG. 19. The same as in Fig. 6, but for a two-band model using $\mu = -1.05t$, $\mu_B B = 0.27t$, the interband hybridization $t_{12} = t$, and the interband spin-orbit coupling $\alpha_{12} = \alpha$.

Z_2 number changes. It suggests that the local density of states in the internal part of the Rashba chain (distant from the Majorana quasiparticles) could be useful for identifying the disorder-induced topological transition.

APPENDIX D: TWO-BAND RASHBA CHAIN

Up to this point we have investigated the Majorana quasiparticles of a strictly one-dimensional chain, where they are created by occupying only the lowest transverse sub-band of atomic nanowire. Since such a condition might be difficult to satisfy in real experiments, we shall address here the influence of disorder on the Majorana states for the simplest multiband system. It has been demonstrated in Refs. [63,64] that a multiband Rashba chain coupled to an s-wave bulk

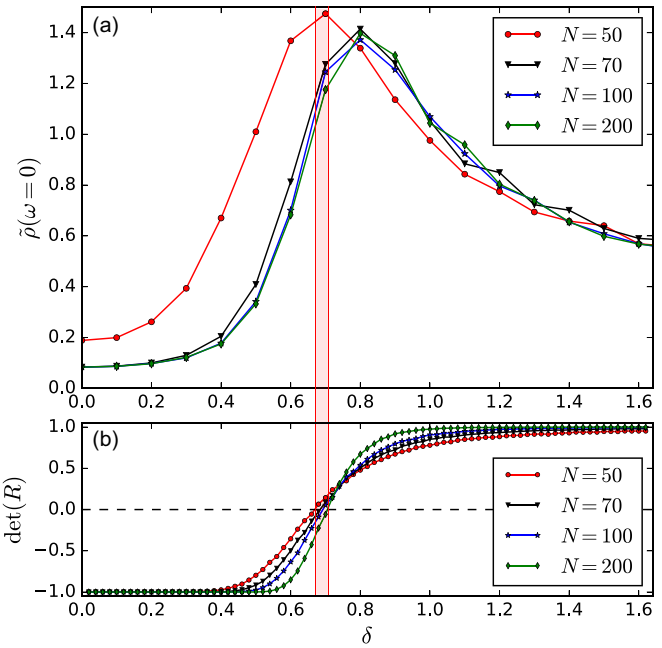

FIG. 20. Geometrically averaged local density of states at central site $i = N/2$ obtained for zero energy within the two-band model with the same model parameters as in Fig. 19.

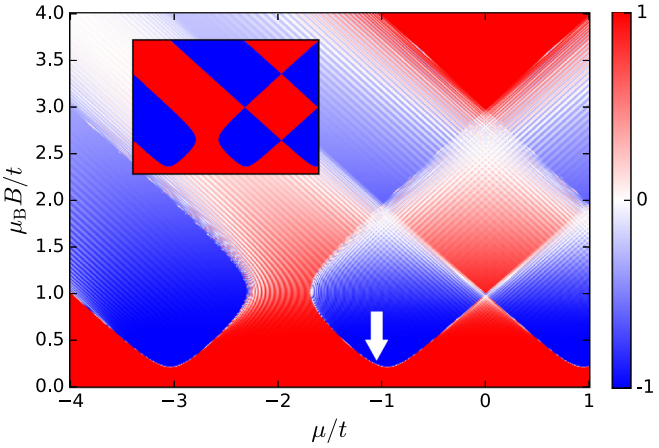

FIG. 21. The same as in Fig. 10, but for a two-band model. The results presented in Figs. 19 and 20 are obtained for the system in topologically nontrivial regime (indicated by the white arrow), that is hardly affected by the finite-size effects.

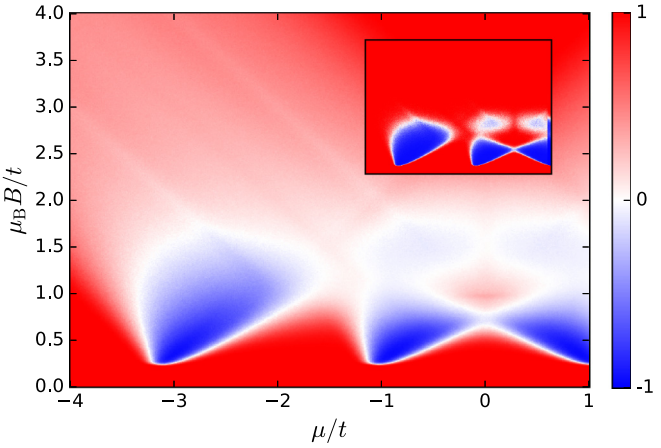

FIG. 22. The same as in Fig. 11(b), but for a two-band model. Additionally, the inset shows the sign of $\det(R)$ averaged over 10^4 disorder realizations.

superconductor can be effectively modeled with two chains, whose coupling depends on external parameters that can be tuned. For studying how robust the Majorana quasiparticles of multiband disordered systems are, we generalize the Hamiltonian (5) to the form

$$\hat{H}_{2b}^{(\mathrm{prox})} = \hat{H}_{\mathrm{chain}}^{(\mathrm{prox})}(\hat{c}) + \hat{H}_{\mathrm{chain}}^{(\mathrm{prox})}(\hat{d}) + t_{12}\sum_{i,\sigma}\hat{c}_{i\sigma}^{\dagger}\hat{d}_{i\sigma} + \mathrm{H.c.} + \alpha_{12}\sum_{i,\sigma\sigma'}[\hat{c}_{i\sigma}^{\dagger}(i\sigma^{x})\hat{d}_{i\sigma'} - \hat{d}_{i\sigma}^{\dagger}(i\sigma^{x})\hat{c}_{i\sigma'}], \quad \text{(D1)}$$

where $\hat{c}_{i\sigma}$ ($\hat{d}_{i\sigma}$) are annihilation operators for electrons in chain 1 (2) described by Hamiltonians $\hat{H}_{\mathrm{chain}}^{(\mathrm{prox})}(\hat{c})$ [$\hat{H}_{\mathrm{chain}}^{(\mathrm{prox})}(\hat{d})$]. The model parameters are tuned to allow for emergence of the Majorana quasiparticle. Our results are presented in Figs. 19 and 20.

One can see that dependence of the local density of states on disorder is almost exactly the same as in the one-band model. Again, the maximum of $\rho(\omega = 0)$ in the central part of the chain coincides with the critical disorder δ^*. This suggests that in the multiband case δ^* corresponds to transition between the topologically nontrivial and trivial phases.

To confirm this observation we calculated the $\mathbb{Z}_2$ topological quantum number, following the procedure described in Sec. III C. In the present case the scattering matrix [Eq. (8)] was composed of 8×8 blocks R, R', T, T' expressed in the basis given by vectors $(\hat{c}_{i\uparrow}^{\dagger}, \hat{c}_{i\downarrow}^{\dagger}, \hat{c}_{i\downarrow}, -\hat{c}_{i\uparrow}, \hat{d}_{i\uparrow}^{\dagger}, \hat{d}_{i\downarrow}^{\dagger}, \hat{d}_{i\downarrow}, -\hat{d}_{i\uparrow})$. Numerical product of these matrices is even more unstable than for the one-band model case, but fortunately the method proposed in Ref. [54] helps to obtain reliable results. Figure 21 shows $\det(R)$ for the uniform atomic chains comprising 70 and 500 lattice sites.

Influence of the disorder is presented in Fig. 22. By comparing it with Fig. 11(b) we notice that the topologically nontrivial region is in both (one- and two-band) models quite similar. Figures 20(a) and 20(b) indicate that the disorder-induced topological transition coincides with the maximum of the local density of states (at zero energy) in a central site of the atomic chain.

[1] A. Y. Kitaev, Unpaired Majorana fermions in quantum wires, Phys. Usp. **44**, 131 (2001).
[2] N. Read and D. Green, Paired states of fermions in two dimensions with breaking of parity and time-reversal symmetries and the fractional quantum Hall effect, Phys. Rev. B **61**, 10267 (2000).
[3] G. Volovik, Fermion zero modes on vortices in chiral superconductors, JETP Lett. **70**, 609 (1999).
[4] L. Fu and C. L. Kane, Superconducting Proximity Effect and Majorana Fermions at the Surface of a Topological Insulator, Phys. Rev. Lett. **100**, 096407 (2008).
[5] Y. Tanaka, T. Yokoyama, and N. Nagaosa, Manipulation of the Majorana Fermion, Andreev Reflection, and Josephson Current on Topological Insulators, Phys. Rev. Lett. **103**, 107002 (2009).
[6] Y. Oreg, G. Refael, and F. von Oppen, Helical Liquids and Majorana Bound States in Quantum Wires, Phys. Rev. Lett. **105**, 177002 (2010).
[7] R. M. Lutchyn, J. D. Sau, and S. Das Sarma, Majorana Fermions and a Topological Phase Transition in Semiconductor-Superconductor Heterostructures, Phys. Rev. Lett. **105**, 077001 (2010).
[8] T. P. Choy, J. M. Edge, A. R. Akhmerov, and C. W. J. Beenakker, Majorana fermions emerging from magnetic nanoparticles on a superconductor without spin-orbit coupling, Phys. Rev. B **84**, 195442 (2011).
[9] M. Wimmer, A. R. Akhmerov, M. V. Medvedyeva, J. Tworzydło, and C. W. J. Beenakker, Majorana Bound States Without Vortices in Topological Superconductors with Electrostatic Defects, Phys. Rev. Lett. **105**, 046803 (2010).

[10] P. San-Jose, E. Prada, and R. Aguado, ac Josephson Effect in Finite-Length Nanowire Junctions with Majorana Modes, Phys. Rev. Lett. **108**, 257001 (2012).

[11] J. D. Sau and S. Das Sarma, Realizing a robust practical Majorana chain in a quantum-dot-superconductor linear array, Nat. Commun. **3**, 964 (2012).

[12] I. C. Fulga, A. Haim, A. R. Akhmerov, and Y. Oreg, Adaptive tuning of Majorana fermions in a quantum dot chain, New J. Phys. **15**, 045020 (2013).

[13] L. Dai, W. Kuo, and M. C. Chung, Extracting entangled qubits from Majorana fermions in quantum dot chains through the measurement of parity, Sci. Rep. **5**, 11188 (2015).

[14] M. Sato and S. Fujimoto, Topological phases of noncentrosymmetric superconductors: Edge states, Majorana fermions, and non-Abelian statistics, Phys. Rev. B **79**, 094504 (2009).

[15] L. Jiang, T. Kitagawa, J. Alicea, A. R. Akhmerov, D. Pekker, G. Refael, J. I. Cirac, E. Demler, M. D. Lukin, and P. Zoller, Majorana Fermions in Equilibrium and in Driven Cold-Atom Quantum Wires, Phys. Rev. Lett. **106**, 220402 (2011).

[16] J. Alicea, New directions in the pursuit of Majorana fermions in solid state systems, Rep. Prog. Phys. **75**, 076501 (2012).

[17] M. Leijnse and K. Flensberg, Introduction to topological superconductivity and Majorana fermions, Semicond. Sci. Technol. **27**, 124003 (2012).

[18] T. D. Stanescu and S. Tewari, Majorana fermions in semiconductor nanowires: Fundamentals, modeling, and experiment, J. Phys.: Condens. Matter **25**, 233201 (2013).

[19] C. W. J. Beenakker, Search for Majorana fermions in superconductors, Annu. Rev. Condens. Matter Phys. **4**, 113 (2013).

[20] S. R. Elliot and M. Franz, Colloquium: Majorana fermions in nuclear, particle, and solid-state physics, Rev. Mod. Phys. **87**, 137 (2015).

[21] M. Sato and Y. Ando, Topological superconductors, Rep. Prog. Phys. (to be published), arXiv:1608.03395.

[22] V. Mourik, K. Zuo, S. M. Frolov, S. R. Plissard, E. P. A. M. Bakkers, and L. P. Kouwenhoven, Signatures of Majorana fermions in hybrid superconductor-semiconductor nanowire devices, Science **336**, 1003 (2012).

[23] S. Nadj-Perge, I. K. Drozdov, J. Li, H. Chen, S. Jeon, J. Seo, A. H. MacDonald, B. A. Bernevig, and A. Yazdani, Observation of Majorana fermions in ferromagnetic atomic chains on a superconductor, Science **346**, 602 (2014).

[24] R. Pawlak, M. Kisiel, J. Klinovaja, T. Maier, S. Kawai, T. Glatzel, D. Loss, and E. Meyer, Probing atomic structure and Majorana wave functions in mono-atomic Fe chains on superconducting Pb surface, Quantum Info. **2**, 16035 (2016).

[25] M. Ruby, F. Pientka, Y. Peng, F. von Oppen, B. W. Heinrich, and K. J. Franke, End States And Subgap Structure in Proximity-Coupled Chains of Magnetic Adatoms, Phys. Rev. Lett. **115**, 197204 (2015).

[26] H.-H. Sun, K.-W. Zhang, L.-H. Hu, C. Li, G.-Y. Wang, H.-Y. Ma, Z.-A. Xu, C.-L. Gao, D.-D. Guan, Y.-Y. Li, C. Liu, D. Qian, Y. Zhou, L. Fu, S.-C. Li, F.-C. Zhang, and J.-F. Jia, Majorana Zero Modes Detected with Spin Selective Andreev Reflection in the Vortex of a Topological Superconductor, Phys. Rev. Lett. **116**, 257003 (2016).

[27] T. D. Stanescu, R. M. Lutchyn, and S. Das Sarma, Majorana fermions in semiconductor nanowires, Phys. Rev. B **84**, 144522 (2011).

[28] P. W. Brouwer, M. Duckheim, A. Romito, and F. von Oppen, Topological superconducting phases in disordered quantum wires with strong spin-orbit coupling, Phys. Rev. B **84**, 144526 (2011).

[29] P. W. Brouwer, M. Duckheim, A. Romito, and F. von Oppen, Probability Distribution of Majorana End-State Energies in Disordered Wires, Phys. Rev. Lett. **107**, 196804 (2011).

[30] D. Rainis, L. Trifunovic, J. Klinovaja, and D. Loss, Towards a realistic transport modeling in a superconducting nanowire with Majorana fermions, Phys. Rev. B **87**, 024515 (2013).

[31] W. DeGottardi, D. Sen, and S. Vishveshwara, Majorana Fermions in Superconducting 1D Systems Having Periodic, Quasiperiodic, and Disordered Potentials, Phys. Rev. Lett. **110**, 146404 (2013).

[32] Y. Hu, Z. Cai, M. A. Baranov, and P. Zoller, Majorana fermions in noisy Kitaev wires, Phys. Rev. B **92**, 165118 (2015).

[33] H.-Y. Hui, J. D. Sau, and S. Das Sarma, Bulk disorder in the superconductor affects proximity-induced topological superconductivity, Phys. Rev. B **92**, 174512 (2015).

[34] B. Pekerten, A. Teker, O. Bozat, M. Wimmer, and I. Adagideli, Disorder-induced topological transitions in multichannel Majorana wires, Phys. Rev. B (to be published), arXiv:1509.00449.

[35] J. Klinovaja and D. Loss, Fermionic and Majorana bound states in hybrid nanowires with non-uniform spin-orbit interaction, Eur. Phys. J. B **88**, 62 (2015).

[36] S. Hoffman, J. Klinovaja, and D. Loss, Topological phases of inhomogeneous superconductivity, Phys. Rev. B **93**, 165418 (2016).

[37] P. Zhang and F. Nori, Majorana bound states in a disordered quantum dot chain, New J. Phys. **18**, 043033 (2016).

[38] Z.-H. Wang, E. V. Castro, and H.-Q. Lin, Effect of disorder in non-uniform hybrid nanowires with Majorana and fermionic bound states, arXiv:1601.05318.

[39] W. S. Cole, J. D. Sau, and S. Das Sarma, Proximity effect and Majorana bound states in clean semiconductor nanowires coupled to disordered superconductors, Phys. Rev. B **94**, 140505(R) (2016).

[40] S. Hegde and S. Vishveshwara, Majorana wave function oscillations, fermion parity switches, and disorder in Kitaev chains, Phys. Rev. B **94**, 115166 (2016).

[41] M. Gibertini, F. Taddei, M. Polini, and R. Fazio, Local density of states in metal-topological superconductor hybrid systems, Phys. Rev. B **85**, 144525 (2012).

[42] Y. Peng, F. Pientka, L. I. Glazman, and F. von Oppen, Strong Localization of Majorana End States in Chains of Magnetic Adatoms, Phys. Rev. Lett. **114**, 106801 (2015).

[43] D. Chevallier, D. Sticlet, P. Simon, and C. Bena, Mutation of Andreev into Majorana bound states in long superconductor-normal and superconductor-normal-superconductor junctions, Phys. Rev. B **85**, 235307 (2012).

[44] R. V. Mishmash, D. Aasen, A. P. Higginbotham, and J. Alicea, Approaching a topological phase transition in Majorana nanowires, Phys. Rev. B **93**, 245404 (2016).

[45] D. Chevallier and J. Klinovaja, Tomography of Majorana fermions with STM tips, Phys. Rev. B **94**, 035417 (2016).

[46] A. Yazdani, Visualizing Majorana fermions in a chain of magnetic atoms on a superconductor, Phys. Scr. **T164**, 014012 (2015).

[47] M. Cheng, R. M. Lutchyn, V. Galitski, and S. Das Sarma, Splitting of Majorana-Fermion Modes Due to Intervortex Tunneling in a $p_x + ip_y$ Superconductor, Phys. Rev. Lett. **103**, 107001 (2009).

[48] S. Das Sarma, J. D. Sau, and T. D. Stanescu, Splitting of the zero-bias conductance peak as smoking gun evidence for the existence of the Majorana mode in a superconductor-semiconductor nanowire, Phys. Rev. B **86**, 220506(R) (2012).

[49] S. Gangadharaiah, B. Braunecker, P. Simon, and D. Loss, Majorana Edge States in Interacting One-Dimensional Systems, Phys. Rev. Lett. **107**, 036801 (2011).

[50] J. Klinovaja and D. Loss, Composite Majorana fermion wave functions in nanowires, Phys. Rev. B **86**, 085408 (2012).

[51] A. V. Balatsky, I. Vekhter, and J.-X. Zhu, Impurity-induced states in conventional and unconventional superconductors, Rev. Mod. Phys. **78**, 373 (2006).

[52] A. R. Akhmerov, J. P. Dahlhaus, F. Hassler, M. Wimmer, and C. W. J. Beenakker, Quantized Conductance at the Majorana Phase Transition in a Disordered Superconducting Wire, Phys. Rev. Lett. **106**, 057001 (2011).

[53] I. C. Fulga, F. Hassler, A. R. Akhmerov, and C. W. J. Beenakker, Scattering formula for the topological quantum number of a disordered multimode wire, Phys. Rev. B **83**, 155429 (2011).

[54] I. Snyman, J. Tworzydło, and C. W. J. Beenakker, Calculation of the conductance of a graphene sheet using the Chalker-Coddington network model, Phys. Rev. B **78**, 045118 (2008).

[55] E. Vernek, P. H. Penteado, A. C. Seridonio, and J. C. Egues, Subtle leakage of a Majorana mode into a quantum dot, Phys. Rev. B **89**, 165314 (2014).

[56] D. A. Ruiz-Tijerina, E. Vernek, L. G. G. V. Dias da Silva, and J. C. Egues, Interaction effects on a Majorana zero mode leaking into a quantum dot, Phys. Rev. B **91**, 115435 (2015).

[57] J. Billy, V. Josse, Z. Zuo, A. Bernard, B. Hambrecht, P. Lugan, D. Clment, L. Sanchez-Palencia, P. Bouyer, and A. Aspect, Direct observation of Anderson localization of matter waves in a controlled disorder, Nature (London) **453**, 891 (2008).

[58] J. Bauer, A. Oguri, and A. C. Hewson, Spectral properties of locally correlated electrons in a Bardeen Cooper Schrieffer superconductor, J. Phys.: Condens. Matter **19**, 486211 (2007).

[59] Y. Yamada, Y. Tanaka, and N. Kawakami, Interplay of Kondo and superconducting correlations in the nonequilibrium Andreev transport through a quantum dot, Phys. Rev. B **84**, 075484 (2011).

[60] A. F. Andreev, Thermal conductivity of the intermediate state of superconductors, Zh. Eksp. Teor. Fiz. **46**, 1823 (1964) [Sov. Phys. JETP **19**, 1228 (1964)].

[61] L. Yu, Bound state in superconductors with paramagnetic impurities, Acta Phys. Sin. **21**, 75 (1965); H. Shiba, Classical spins in superconductors, Progr. Theor. Phys. **40**, 435 (1968); A. I. Rusinov, On the theory of gapless superconductivity in alloys containing paramagnetic impurities, Sov. Phys. JETP **29**, 1101 (1969).

[62] J. Barański and T. Domański, In-gap states of a quantum dot coupled between a normal and a superconducting lead, J. Phys.: Condens. Matter **25**, 435305 (2013).

[63] R. M. Lutchyn, T. D. Stanescu, and S. Das Sarma, Search for Majorana Fermions in Multiband Semiconducting Nanowires, Phys. Rev. Lett. **106**, 127001 (2011).

[64] R. M. Lutchyn and M. P. A. Fisher, Interacting topological phases in multiband nanowires, Phys. Rev. B **84**, 214528 (2011).